Journal of Organometallic Chemistry, 472 (1994) 229–246

The protonation mechanism of metallocenes and [1.1]metallocenophanes

Ulrich T. Mueller-Westerhoff, Thomas J. Haas [1], Gerhard F. Swiegers [2] and Thomas K. Leipert

Department of Chemistry, University of Connecticut, Storrs, CT 06269-3060 (USA)

Received December 17, 1993; in revised form February 15, 1994

Abstract

A study of the protonation and deuteration of [1.1]metallocenophanes has revealed several details of the mechanism of metallocene protonation. In [1.1]ferrocenophane, protonation at both metallocenes is immediately followed by elimination of dihydrogen. The resulting bis-ferrocenium ion is substitutionally inert and no longer takes part in protonation or deuteration. This convenient circumstance permits us to analyze the protonation mechanism in greater detail than monomeric ferrocenes would allow. The reaction of [1.1]ferrocenophanes with deuterated acids leads to partially or completely deuterated rings, depending on their structure and the reaction conditions. The experimental results on ferrocene-containing systems are not compatible with a reaction path in which the incoming electrophile binds first to the iron and then transfers to the ring. Substitution must rather occur by *exo*-attack on the ring, followed by transfer of the proton to the metal and back to either one of the rings. For protonated ferrocene, a rapid equilibrium between ring- and metal-protonated species exists; deuterated acids lead to rapid and complete H/D exchange. In contrast to the protonation of ferrocene, the protonation of ruthenocene occurs at the metal only, without any participation of the Cp rings. Consequently, ruthenocene reacts with deuterated acids without H/D exchange. Studies on [1.1]ferroceno-ruthenocenophane demonstrate the differences in the protonation of these two metallocenes.

Key words: Iron; Ruthenium; Metallocenes; Protonation; Deuteration; Mechanism

1. Introduction and background

Over a period of several years, we have investigated the chemistry of [1.1]metallocenophanes from different angles: studies of the synthesis [1–6], molecular [7–10] and electronic [11–14] structure, conformational properties, [15] redox chemistry, [16] reactivity and functionalization of [1.1]ferrocenophane and of its ruthenocene analogs and the structure of carbocations [17] and carbanions [18] derived from these species produced a number of structural and mechanistic surprises [19]. The reaction of ferrocenophanes with acids was exploited in a catalytic cycle: a polymer-bound ferrocenophane was used in modifying the surface of Si photocathodes as half of a solar cell for the production of hydrogen from water [20]. Knowledge of the detailed mechanism of metallocene protonation and, in particular, of the protonation and hydrogen elimination mechanisms in ferrocenophanes is intimately related to such applications. In spite of this, considerable uncertainty remains about the exact steps involved.

The protonation and, more generally, the electrophilic substitution of the iron group metallocenes has been investigated many times [21–32]. The argumentation centered around the primary step in this reaction and whether or not the electrophile would first coordinate to the metal ("*endo*-attack", path a in Fig. 1) or attach itself to one of the rings ("*exo*-attack", path b of Fig. 1). Elegant early work by Rosenblum *et al.* [22] showed that the latter would be much more likely.

Two very recent publications have addressed the protonation of ferrocene from the experimental [31] and theoretical [32] side. Because these latest results

Correspondence to: Professor U.T. Mueller-Westerhoff.

* Dedicated in friendship to Professor H. Werner on the occasion of his 60th birthday.

[1] Taken in part from the Ph.D thesis of T.J. Haas, University of Connecticut, 1987. Permanent address of TJH: United States Coast Guard Academy, New London, CT 06320, USA.

[2] Taken in part from the Ph.D. thesis of G.F. Swiegers, University of Connecticut, 1991. Present address of GFS: Research School of Chemistry, Australian National University, Canberra, A.C.T. 0200, Australia.

0022-328X/94/$7.00
SSDI 0022-328X(94)24591-6

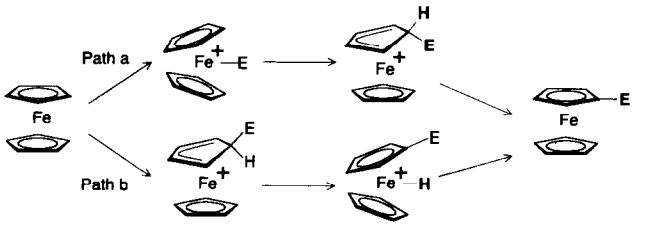

Fig. 1. *Endo* (path a) and *exo* (path b) attack pathways for electrophilic substitution of ferrocene.

again do not agree on the most probable pathway, we present here some of our own work to clarify the mechanism of protonation and deuteration of the metallocenes and metallocenophanes of iron and ruthenium.

The compounds with which we will deal in this paper are ferrocene (**1**), ruthenocene (**2**), the two [1.1]metallocenophanes **3** and **4** of iron and ruthenium, the [1.1]ferrocenophane dimer **5** ([1.1.1.1]ferrocenophane), and its mixed iron–ruthenium analog **6**.

1.1. Some relevant properties of metallocenes and metallocenophanes

The metallocenes have been known for over forty years and need little introduction. A recent review [19] on [1.1]metallocenophanes has summarized most of the work related to this class. We therefore need only discuss a few key properties to bring the present work into focus.

Ferrocene can be reversibly oxidized at low potentials to the deep blue-green paramagnetic monocation, the ferrocenium ion, which is inert to substitution and H/D exchange. A higher potential is required to oxidize ruthenocene, and this oxidation is an irreversible two-electron process which leads to the dication. Both metallocenes act as very weak bases: their complete protonation occurs in strong acids to form metallocenonium ions which are easily oxidized. The acids to be used therefore must be non-oxidizing to avoid formation of the metallocenium ions: concentrated H_2SO_4 protonates ferrocene below 0°C but oxidizes it rapidly at room temperature or above; ruthenocene dissolves in concentrated H_2SO_4 at room temperature and oxidation is slow up to 40°C.

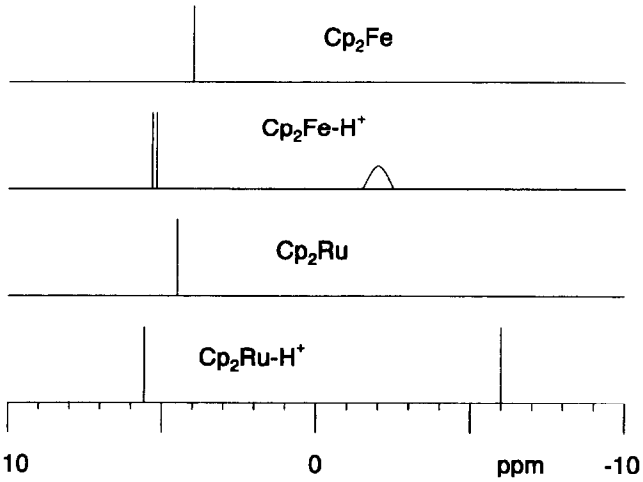

Fig. 2. Schematic representation of the chemical shifts of the neutral metallocenes in CCl_4 and of their protonation products in HBF_3OH.

Several NMR investigations of the diamagnetic protonated species have been reported [23–27]. For protonated ferrocene, often called the ferrocenonium ion, the additional proton has mostly been assumed to reside on the metal, although the protonation of the Cp ligands has been established in interactions with weakly acidic species. The NMR spectrum of ferrocene in boron trifluoride hydrate (HBF_3OH), first reported in 1960 [21] showed the ten ring protons as a doublet ($J \approx 1$ Hz) at 5.2 ppm (compared to 4.1 ppm in ferrocene) and the "hydridic" proton near −2 ppm as a broad signal with no discernible fine structure (Fig. 2). The coupling of the "hydridic" proton with all ring protons was taken as evidence that the proton resides at the metal and that it interacts equally with both rings. We will show in this paper that this is an incomplete and incorrect interpretation.

Ruthenocene in HBF_3OH (Fig. 2) shows no coupling between the ring protons and the hydridic proton: sharp singlets are observed at 5.6 ppm (ring protons) and −6.2 ppm (hydridic proton). The first report [21] noted an integral ratio of these signals (16:1) which corresponded to less than one hydridic proton, and this was taken as evidence for a lesser basicity of ruthenocene as compared to ferrocene. Our own investigations of the NMR spectra of the protonated metallocenes showed clean 10:1 integrals for protonated ferrocene and for ruthenocene.

In analogy to structurally characterized metallocene hydrides such a Cp_2ReH and related systems [33], it

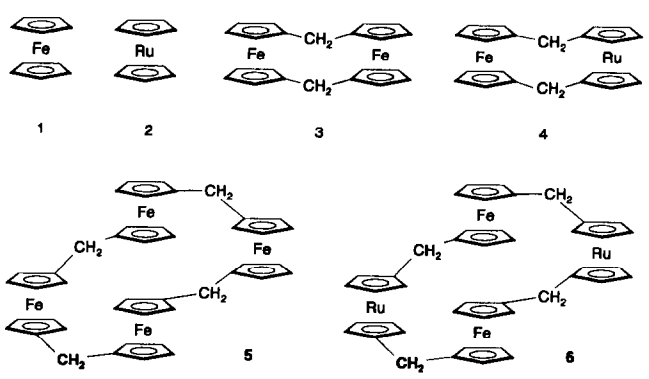

has been assumed that the protonated ferrocene also has the typical bent structure. This is reasonable if we consider that the ligands in ferrocene [34] and in the ferrocenophanes [10,35] are planar and coplanar with a ring–ring distance of ≈ 330 pm. Because this distance is even less than the Van-der-Waals thickness of an aromatic ring, such as the interplanar distance of 340 pm found in crystalline aromatics, it is *a priori* not likely for a proton to fit in without some degree of deviation of the rings from coplanarity to make some room for the additional ligand. The situation could be quantitatively different for ruthenocene, which has a ring–ring distance of 370 pm and thus could accommodate a proton more easily.

Quantum chemical calculations on ferrocene differ in detail, but all agree on the fact that the metal carries a positive charge. A calculation [12] at the INDO level showed a charge of + 1.9 on the iron in neutral ferrocene; the most recent published data [32] show a spread between + 1.16 and 0.29, depending on the computational level; a recent IEHT calculation [36] reduced this charge to + 0.51 as an excellent compromise value. The positive charge makes an attack of electrophiles at the metal unlikely, because more or less severe Coulomb repulsion would have to be overcome whereas the negatively charged ligands would be the more likely point of attack.

The IEHT results for ruthenocene suggest, in complete contrast to ferrocene, a considerable negative charge on the central metal [36]. Although several accepted parameter sets for ruthenium are currently in use and the results therefore are more ambiguous than those for ferrocene, the existence of some negative charge on ruthenium makes direct attack of an electrophile a very plausible route.

The IEHT calculations also provide a ready explanation for the differences in oxidation potential and in the oxidation process of the two metallocenes (*vide supra*). As shown in Fig. 3, the 3_{dz2} AO is the HOMO in ferrocene, losing and regaining an electron upon oxidation and reduction. In ruthenocene, the 4_{dz2} AO lies below the degenerate ligand π-MOs. Loss of one electron is accompanied by Jahn–Teller splitting which raises the energy of the unpaired electron above the original MO level. The second electron therefore is more easily lost than the first, which results in the observed two-electron oxidation.

The pitfalls of applying more sophisticated quantum chemical methods to ferrocene were already documented by Park and Amlöf [37]. Understandably, the most recent attempt [32] to decide between the *exo*- and *endo*-pathways is inconclusive: at the HF level, *exo* attack was favored whereas a MP2 calculation showed the *endo* pathway to be preferred. It appears that the less sophisticated methods are better suited to mimic the experimental facts and that *exo* attack is favored for ferrocene and *endo* attack for ruthenocene. All theoretical methods agree in one important detail: when bound to the metal, the proton transfers almost all of its charge to the metallocene and this species is best described as having an almost neutral hydrogen atom attached to a ferrocenium system.

The mechanistic question of *exo vs. endo* attack was also investigated theoretically for [1.1]ferrocenophane at the INDO level [14]. This study found ring protonation to be energetically favored over metal protonation as the first reaction step, but it did not rule out the possibility that direct protonation at the metal sites could be an alternate low energy pathway, if the optimized geometries were different from those used in the calculation.

1.2. [1.1]Metallocenophanes

The [1.1]metallocenophanes can contribute valuable information to the problem of the exact pathway of metallocene substitution reaction, because linking metallocenes in this manner produces systems with electronically non-interacting metallocenes in which the metal centers are nevertheless held closely together. This introduces reaction pathways which are not possible in mononuclear systems.

To discuss their structure and reactivity, we will focus on [1.1]ferrocenophane (**3**, abbreviated as FCP), the by far best investigated example of this class. One might assume that this compound should exist in two isomeric forms or as a mixture thereof: the two methylene bridges in FCP should either be on the same side (*syn* form, *syn*-**3**) or on opposite sides of the two ferrocenes (*anti* form, *anti*-**3**). In both forms the protons in the inner α-position would be severely crowding each other.

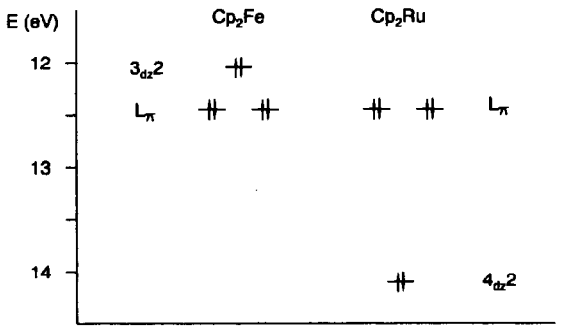

Fig. 3. Simplified MO diagram showing only the highest occupied MOs of ferrocene and ruthenocene.

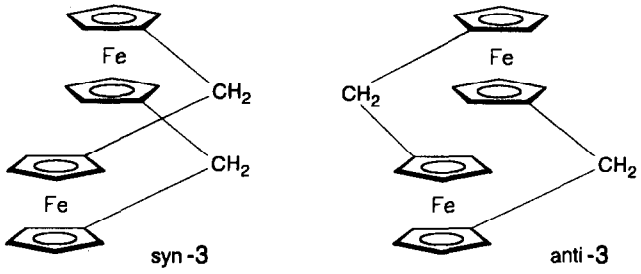

Dreiding models demonstrate that an undistorted *anti* form is totally rigid and cannot relieve the overcrowding, unless the Cp ligands undergo a major tilt to a non-coplanar structure [35,38]. Only the *syn* form is flexible enough to relieve all steric problems. This flexibility is directly linked to the ease with which the two cyclopentadienyl ligands can rotate with respect to each other, although this motion now is coupled by the methylene links to the other ferrocene. This degree of freedom lets the molecule undergo synchronized motion from one *syn* conformation to its mirror image [3,39]. This flexibility can be diminished or even suppressed by substituents either on the rings [15] or on the bridges [39,40].

The *syn* conformation of FCP and its Ru analogs has been confirmed by X-ray crystallography [10]. The Fe–Fe distance in the crystal is 4.6 Å, but molecular models show that at the saddle point of the *syn–syn* exchange this distance may shrink to 3.6 Å. Single crystals of the mixed Fe–Ru system were also investigated: a very similar structure was found, but with the expected dissymmetry imposed by the different ring–ring distances of ferrocene and ruthenocene (3.3 *vs.* 3.7 Å).

As will be discussed below in detail, protonation of [1.1]ferrocenophane by strong acids leads to hydrogen evolution and the ferrocenophane dication. Since the metallocenophane dications are reaction products of the protonation, the oxidation potentials of metallocenophanes, given in Table 1, are a direct link between protonation and the reactivity of the protonated species. For the two [1.1]metallocenophanes in this study, we find the typical behavior, as predictable from the properties of the isolated metallocenes [16].

TABLE 1. Redox potentials of the metallocenes and metallocenophanes **1** to **4**. Data were obtained from cyclic voltammetry in benzonitrile/Bu_4NBF_4 *vs.* NaSCE at 50 mV s^{-1}. The E° values are the standard potentials; ΔE is the difference in peak potentials; e indicates the number of electrons involved in this step.

	$E1$	ΔE	e	$E2$	ΔE	e
1	500	60	1	–	–	–
2	920	500	2	–	–	–
3	410	80	1	610	80	1
4	400	80	1	920	500	2

Abstraction of a hydride from one of the bridges in [1.1]ferrocenophane, using triphenylcarbenium tetrafluoroborate as the hydride acceptor, leads to the BF_4 salt of a carbocation as a stable, crystalline species [17]. Its full spectroscopic characterization is of importance in the protonation studies, because we will see that it also derives from the FCP dication by loss of a proton. The carbocation can be regarded at as a special case of α-ferrocenyl carbocations, in that the two *cis*-fixed ferrocenes most efficiently stabilize the positive charge. Mössbauer spectroscopy showed that each of the ferrocenes takes up one third of the positive charge so that only one third of it is left at the bridge carbocation center [17].

1.3. The protonation of [1.1]ferrocenophanes

From the above properties of ferrocene and ferrocenophanes, it seems likely that the latter reacts with acids such as HBF_3OH (regardless of the exact protonation mechanism) to form a diprotonated species. This was indeed the expectation when this experiment was first carried out by Bitterwolf and Ling [27], who, however, instead observed a rapid reaction with evolution of a gas and the formation of a deep blue, paramagnetic solution. The authors correctly identified the gas as hydrogen and the blue solution as that of the bis-ferrocenium ion. Bitterwolf [28] has carried out this reaction with DBF_3OD and found that the gas evolved from this system was comprised of mainly H_2 and HD with smaller amounts of D_2. Such an observation implicates the participation of the [1.1]ferrocenophane ring hydrogens (*via exo*-attack) in the hydrogen evolution step. If hydrogen evolution would occur only by protonation directly at the metal, the gas evolved would be only D_2.

The reaction of [1.1]ferrocenophane with HBF_3OH clearly must involve a stepwise double protonation. Because the protonation of metallocenes is reversible, it is likely that many protonation–deprotonation steps occur on either one of the rings before both ferrocenes are protonated at the same time. As soon as the diprotonated [1.1]ferrocenophane is formed, an irreversible regime is entered: the second protonation is rapidly followed by elimination of a dihydrogen molecule and the resulting bis-ferrocenium system no longer reacts with the acid.

Hydrogen elimination can only occur because the [1.1]ferrocenophane dication is energetically easily accessible and the overall reaction is a downhill process. If in related systems a dication does not exist, or if it is a relatively high energy species, hydrogen elimination from the diprotonated species should not be possible.

Reduction of the dication by solutions of standard reducing agents leads to recovery of [1.1]ferrocenophane in close to quantitative yields. Addition of elemental Pb or Sn to the undiluted acid leads to slow dissolution of the metals. This is significant, because neither of these metals react with HBF_3OH in the absence of the [1.1]ferrocenophane: although they are rather electropositive, Pb and Sn possess a considerable overpotential to hydrogen evolution and therefore can be placed in HBF_3OH indefinitely without any reaction occurring. That they do react in the presence of FCP means that the latter acts as a catalyst in the reaction of these metals with the acid. Indeed this is plausible, because the metal is a strong reducing agent and can react with the [1.1]ferrocenophane dication with transfer of two electrons ($Pb + FCP^{2+} \rightarrow Pb^{2+} +$ FCP). The neutral FCP can re-enter a catalytic cycle until all of the metal is dissolved.

The electrons generated at the surface of an irradiated *p*-type Si semiconductor also are of sufficient energy to reduce the dication to the neutral species, but their direct reaction with protons to form dihydrogen is kinetically inhibited by a significant overpotential. Therefore, Si photocathodes cannot be used, *e.g.* in solar cells, without some type of surface modification. [1.1]Ferrocenophane acts as an efficient catalyst in this case as well [20].

A complete interpretation of the protonation mechanism of [1.1]ferrocenophane and its derivatives certainly is most desirable. It should provide insight into the roles of the metal centers, the Cp rings, and the methylene bridges. The failure to observe any hydrogen evolution from ferrocene or from diferrocenyl methane indicates that protonation at both metal centers is not a sufficient prerequisite for hydrogen evolution, but that the forced proximity of the two metal centers in FCP and its analogs is an indispensable asset. The flexibility of the FCP system also is a prerequisite: no efficient hydrogen evolution was observed with [0.0]ferrocenophane (bis-fulvalene-diiron). In protonated binuclear ferrocene molecules such as diferrocenyl methane, Coulombic repulsion prevents the two protons from coming into bonding distance and to allow the formation of a dihydrogen molecule. None of them are hydrogen generation catalysts, although they are slowly oxidized in acidic solution when exposed to air.

Since formation of protonated ferrocenes probably involves a bent structure with increased strain in the molecule, we may consider how this affects the [1.1]ferrocenophane case. Models indicate a moderate amount of strain in the ferrocenophane framework upon single protonation of one of the metal centers and substantially more strain in the diprotonated molecule. Relief

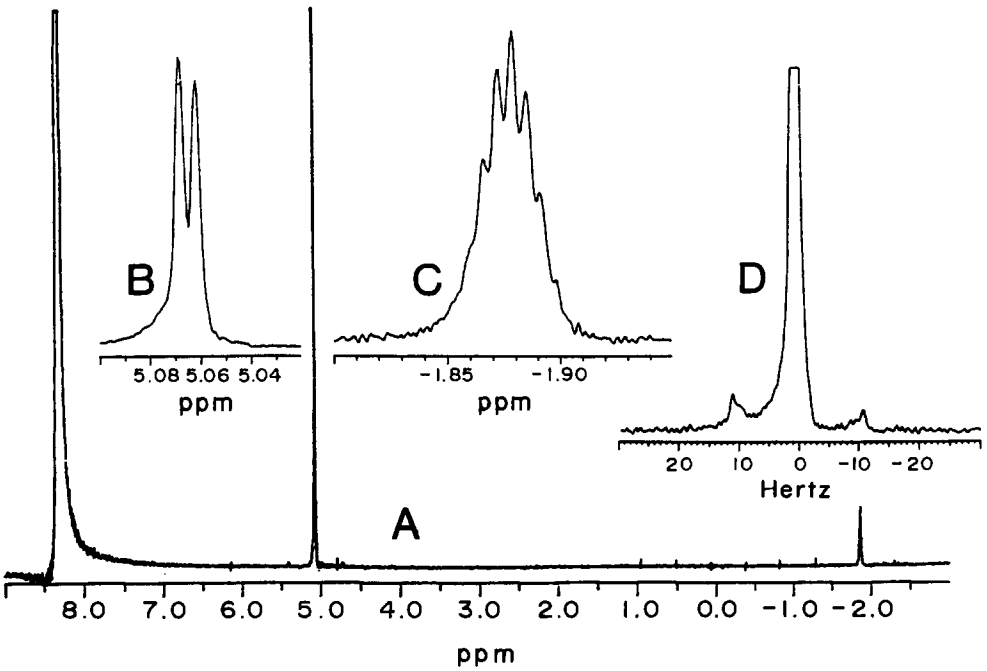

Fig. 4. Proton NMR spectrum of Cp_2Fe in HBF_3OH. Because the sample contains no deuterium, the acid/H_2O peak was defined as 8.30 ppm; no shimming of the FID was attempted. A: The full spectrum with enlarged portions B (Cp–H signal) and C (hydride signal); D: proton decoupled signal (irradiation at 5.1 ppm) of the hydride peak; note the satellites due to ^{57}Fe–H coupling.

of this strain may be an additional driving force in the hydrogen evolution step. Ring or bridge substituents will influence the degree of strain and thus most likely retard the reaction. Hillman *et al.* [40] have observed that for sterically restrained FCP derivatives, such as 3,3'-trimethylene[1.1]ferrocenophane, the rate of gas evolution is slower. Our own work on bridge-substituted FCP derivatives also has shown that the protonation rates are reduced by the introduction of alkyl substituents. These results will be reported separately.

Hillman *et al.* [41] have also reported the results of a kinetic study of the formation of dihydrogen from the parent FCP and strong acids. Based on electrochemical studies, they propose that the elimination of dihydrogen is the rate-determining step. They concede that other mechanisms are possible, and suggest that the protonation of the iron may be preceded by protonation of a ring carbon. Involvement of the methylene bridges was also considered. However, these studies suffer from an erroneous identification of the reaction products, as will be shown below.

To arrive at a consistent explanation would obviously clarify the misunderstandings in the current literature about this protonation mechanism. Our study of the metallocenes and metallocenophanes **1–4** attempts to do just that.

2. Experimental results and discussion

To probe the details of the reaction of the [1.1]metallocenophanes and their metallocene parents with non-oxidizing acids, a series of protonation and deuteration studies was undertaken. These studies used either HBF_3OH (H_2O saturated with BF_3) or DBF_3OD (D_2O saturated with BF_3) as the acid. The degree and regioslectivity of deuteration and protonation was studied by mass spectra and ^1H- and ^2H-NMR.

2.1. Reactions of ferrocene and perdeuterated ferrocene with acids

The reaction of ferrocene with HBF_3OH has been studied many times, and we originally repeated it only for the sake of calibration. Because oxidation of ferrocene to ferrocenium ion occurs instantaneously in the presence of air, the reaction must be conducted in an inert atmosphere. The ^1H-NMR spectrum in HBF_3OH at 270 MHz showed two peaks in the ratio 10:1 at 5.06 ppm (doublet, $J = 1.75 \pm 0.1$ Hz) and -1.88 ppm (broad), relative to the acid peak, which was fixed at 8.30 ppm. Under strict anaerobic conditions it was possible to resolve the hydride peak at -1.88 ppm to reveal a fine structure with a 1.75 Hz splitting (Fig. 4C). Although the outermost peaks were not observable, the peak distribution is typical for an undecet in which the three center peaks are expected to be > 200 times as intense as the outermost peaks (symmetrical signal with peak ratios of 1:10:42:117:210:252). A decoupling experiment provided an interesting result. Irradiating the peak at 5.1 ppm led to the expected collapse of the multiplet at -1.9 ppm to a singlet, but the singlet also showed weak satellite peaks at ± 10.8 Hz with approximately 1.5% of the intensity of the main signal (Fig. 3D). This intensity corresponds closely to the one expected for the 2.1% natural abundance of the ^{57}Fe isotope, and were therefore attribute the satellites to the first direct observation of Fe–H coupling. The observed J(Fe–H) of 21.6 Hz may well be a reduced value, because of rapid exchange between ring- and metal-bound proton exchange (*vide infra*). The spectrum of ferrocene in DBF_3OD showed no proton signal in the 5–6 ppm range, but a visible increase in the acid signal at 8.30 ppm. This result indicates that rapid and complete deuteration of the Cp rings had occurred in accord with previous reports. The d_{10}-ferrocene was recovered by adding water to the yellow solution.

The perdeuterated ferrocene was added to HBF_3OH. Its spectrum was recorded, and identified as that of the well-known protonated ferrocene: the ferrocene doublet at 5.1 ppm and the Fe–H signal at -2 ppm indicated that complete and rapid reversal of the deuteration had occurred.

2.2. Ruthenocene

When crystalline ruthenocene was added to DBF_3OD, it rapidly dissolved. The spectrum of ruthenocene in the acid recorded 2 min after addition gave two signals: a singlet at 8.50 ppm (acid peak) and a single peak at 5.60 ppm. The spectrum of the same sample was rerun after 5, 10, 20, and 60 min without change in the signal position or integral. Workup of this reaction mixture the same way as with ferrocene gave back ruthenocene. The mass spectrum showed that no deuteration of the Cp rings had occurred.

The downfield shift of the Cp signal from 4.60 ppm in $CDCl_3$ to 5.20 ppm in DBF_3OD is due to the positive charge of the protonated species, analogous to the ferrocene case. We thus assume that ruthenocene is protonated by direct attack at the metal without any apparent involvement of the Cp rings.

Although the protonated ruthenocene is much less sensitive to oxidation than protonated ferrocene, the reaction must be carried out under inert gas to prevent the NMR signals from broadening. The solution of non-oxidized ruthenocene remains pale yellow. The solution of oxidized ruthenocene is yellow/green.

2.3. The mechanism of metallocene protonation

The spectra of protonated ferrocene and ruthenocene were shown in Figs. 2 and 4. We noted the sharp singlets in the ruthenocene case and the coupling between the ring protons and the hydridic proton in the case of ferrocene giving rise to a ring proton doublet and an undecet for the hydridic proton. A further observation is that the sharp signal of the hydridic proton on ruthenocene appears at considerably higher field than the broadened signal of the hydridic proton on ferrocene. We can interpret these results in a consistent way by considering the completely different nature in which the rings are involved in the protonation of these two metallocenes.

The ruthenocene case is simple and corresponds to the classical picture: ruthenocene indeed is protonated by direct attack of the proton on the metal and the rings are not directly involved in this reactions. They may tilt out of the way of the proton, but the larger ring–ring distance in ruthenocene as compared to ferrocene makes this less of a necessity in this case. The absence of any coupling between hydridic and ring protons and the lack of H/D exchange support this picture. An additional argument comes from IEHT calculations [15]. In ruthenocene the metal carries a negative charge and the ligands possess a partial positive charge. This favors protonation on the metal and inhibits protonation at or proton transfer to the ligands.

For protonated ferrocene, all indications point to a direct and continuous involvement of the rings in a dynamic process in which the proton rapidly moves between Fe–H and Cp-ring C–H bonding, illustrated in Fig. 5 for the case of deuteration. The incoming H^+ (or D^+) approaches the ferrocene molecule from the outside of one of the rings and attaches itself to one of the carbon atoms of this ring. This results in a structure in which a cyclopentadiene is coordinated to a $CpFe^+$ fragment. The endo proton transfers to the iron and then can rapidly shuttle back and forth between the iron and any one carbon of either ring. Eventually it is lost to the acid solvent from one of the rings. The principle of microscopic reversibility should forbid that the proton is lost to the solvent from the Fe–H site so that the deprotonation must occur from one of the ring positions. We should note that this is a rapid equilibrium, and that assuming the existence of an "agostic" hydrogen would not fit the experimental data, unless we would postulate the existence of an equilibrium between ten agostic positions — which would be a semantic rather than real differentiation.

This interpretation is consistent with all the experimental data. It explains the high rate and the completeness of deuteration in deuterated acid and it also permits us to understand the NMR data in detail. The appearance of the broadened undecet signal for the hydridic proton at −2 ppm compared to −6 ppm in ruthenocene points to an average chemical shift in protonated ferrocene, weighted between the hydridic position (near −6 ppm) and the CH_2 position (near +2 ppm) on the Cp ring. Since this is a kinetic phenomenon, we should be able to observe a temperature dependence of the NMR spectrum. Unfortunately, the acids HBF_3OH and DBF_3OD show high viscosity already at room temperature and solidify to a glass on cooling, which discourages NMR experiments at lower temperature.

The alternate mechanism, protonation at the Fe atom and subsequent exchange with the rings would not explain the experimental facts if we adhere to the principle of microscopic reversibility: in a deuteration experiment we should not see any H/D exchange. The reasoning is as follows: even if an Fe–D → C–D transfer equilibrium exists, the deuterium will always be in the *endo* position of the ring and, as the only species available to transfer back to the iron, it — and not a proton — will return to the iron, the only site from which it may be lost to the solvent. As indicated in the Introduction, the results from IEHT and INDO calculations, specifically the presence of a positive charge on the iron atom in ferrocene, make protonation *via* direct attack on iron unlikely for Coulomb repulsion reasons.

In summary: it is evident that ferrocene is protonated by *exo*-attack in the rings and that a rapid exchange of the additional proton between all ten ring positions is possible through the intermediacy of a Fe–H bonded species. By contrast, in ruthenocene the

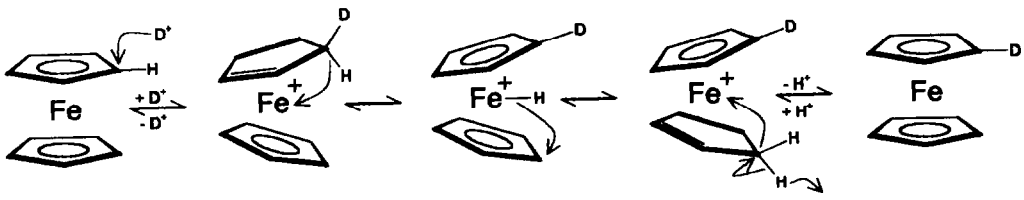

Fig. 5. The mechanism of ferrocene protonation and of the dynamic process in protonated ferrocene.

proton attaches itself to the metal and remains there. This observation has the implication that similar differences should be effective in substitution reactions using electrophiles other than a proton or a deuteron. Our results must leave this question open: although our results tend to imply *exo* attack for other electrophiles as well, the statement that all electrophilic substitutions on ferrocene must proceed *via exo* attack would be unwarranted.

2.4. Protonation and deuteration of [1.1]ferrocenophane

When a batch of four grams of crystalline [1.1]ferrocenophane was added to HBF_3OH, it dissolved rapidly and hydrogen evolution was complete within a few seconds. Measurement of the volume of gas evolved confirmed that one mole of dihydrogen was produced per mole of [1.1]ferrocenophane. Addition of water and reduction by $NaBH_4$ produced the unchanged starting material.

The same reaction was carried out on a very small scale in a quartz cuvette to record the visible spectrum of the initial reaction product. Three peaks were observed at 645, 560, and 470 nm. These typical ferrocenium ion absorptions characterize the blue species as the [1.1]ferrocenophane dication. Upon addition of a few drops of water the intensity of the three ferrocenium ion peaks diminished at the expense of a broad new peak at 740 nm. This is the typical absorption of the ferrocenophane carbocation **8** and identical in every respect to the spectrum of a sample generated from [1.1]ferrocenophane by abstraction of a hydride using triphenyl-carbenium tetrafluoroborate as the hydride acceptor [17].

ton acceptor in this reaction, the dication is stable only in anhydrous solvents or in concentrated acids. Once a proton is lost from the bridge, the resulting monocation **7** relaxes to its more stable resonance form **8**, in which the iron atoms have taken up two thirds of the positive charge [17]. We have to note that any type of normal work-up of the [1.1]ferrocenophane reactions with acids will involve **8** as the primary intermediate whenever the acid is diluted as a first step. The deep blue-green solutions of the carbocation can be converted back to the ferrocenophane by supplying a hydride, which we routinely do by adding $NaBH_4$.

In the reactions of the two isomeric (*exo–exo* and *exo–endo*) bridge-substituted dimethyl[1.1]ferrocenophanes, a closer look at the reaction products revealed two important pieces of information about the mechanism of this deprotonation step and about the reduction of the carbocations by a hydride source to lead back to the starting materials: (i) the two carbocations are not identical and (ii) the recovered dimethyl[1.1]ferrocenophanes have retained their stereochemistry [42]. The consequences of these observations together with the effects of bridge substituents on the rate of protonation and hydrogen evolution will be reported separately in detail.

The formation of the stable carbocation **8** when the concentrated acids (HBF_3OH or DBF_3OD) are diluted with water or when the reaction is carried out in more dilute media [41] is the driving force for a side reaction which removes the ferrocenophane from the existing equilibria. Reactions of [1.1]ferrocenophane in more dilute acid systems certainly lead to the carbocation as

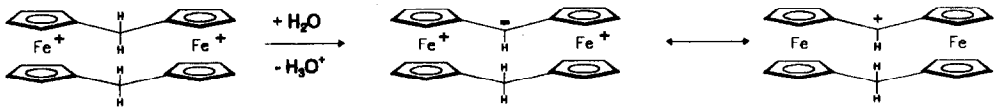

7 8

The formation of the carbocation **8** is easily understood. The presence of two positive charges in the dication increases the acidity of the bridge protons significantly, so that deprotonation can occur even with weak bases. Because water is a sufficiently strong proton acceptor in this reaction, the dication is stable only in anhydrous solvents or in concentrated acids. Once a proton is lost from the bridge, the resulting monocation **7** relaxes to its more stable resonance form **8**, in which the iron atoms have taken up two thirds of the positive charge [17]. We have to note that any type of normal work-up of the [1.1]ferrocenophane reactions with acids will involve **8** as the primary intermediate whenever the acid is diluted as a first step. The deep blue-green solutions of the carbocation can be converted back to the ferrocenophane by supplying a hydride, which we routinely do by adding $NaBH_4$.

In the reactions of the two isomeric (*exo–exo* and *exo–endo*) bridge-substituted dimethyl[1.1]ferrocenophanes, a closer look at the reaction products revealed two important pieces of information about the mechanism of this deprotonation step and about the reduction of the carbocations by a hydride source to lead back to the starting materials: (i) the two carbocations are not identical and (ii) the recovered dimethyl[1.1]ferrocenophanes have retained their stereochemistry [42]. The consequences of these observations together with the effects of bridge substituents on the rate of protonation and hydrogen evolution will be reported separately in detail.

The formation of the stable carbocation **8** when the concentrated acids (HBF_3OH or DBF_3OD) are diluted with water or when the reaction is carried out in more dilute media [41] is the driving force for a side reaction which removes the ferrocenophane from the existing equilibria. Reactions of [1.1]ferrocenophane in more dilute acid systems certainly lead to the carbocation as the major reaction product instead of the dication. In the study by Hillman *et al.* of [1.1]ferrocenophane protonation [41], experiments in acidic media of varying strength were carried out, but the role of the carbocation, which we demonstrated above and whose

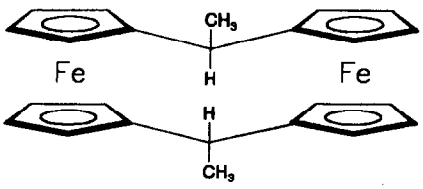

exo-exo

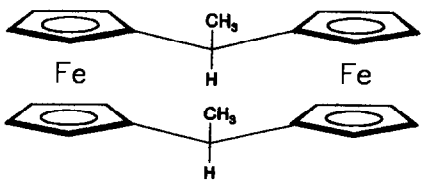

exo-endo

presence was indicated in that work as well by a strong absorption at 750 nm, was not considered.

When solid [1.1]ferrocenophane was added to DBF_3OD, immediate dissolution, gas evolution and formation of a deep blue solution were again observed. The solution was diluted with water, producing a green solution. The electronic spectrum of the green solution showed a broad band at 740 nm, consistent with that of the carbocation. Reduction by $NaBH_4$(aq) produced a yellow solution, from which a yellow crystalline solid was obtained. ^{1}H-NMR, ^{2}H-NMR, and mass spectroscopy showed that significant H/D exchange had occurred on the FCP rings but not on the methylene bridge. The ^{1}H-NMR spectrum gave signals for the bridge protons at 3.53 ppm and the ferrocene protons at 4.32 ppm and 4.16 ppm all with approximately (within 5%) the same integral. This indicated an approximately 50% loss of ring protons by H/D exchange. The ^{2}H-NMR confirmed that only the ring protons were involved in this exchange: only one broad peak at 4.31 ppm was observed. The mass spectrum showed a Gaussian-like distribution of peaks from d_0 to d_{16} with the main peak at m/e 404, denoting the incorporation of, on the average, eight deuterium atoms for hydrogens. The MS and NMR data together indicate that the exchange occurs equally at all ring positions.

To examine whether the extent of the deuteration would change if the reaction was allowed to proceed for a longer period of time, the reaction was carried out as before but worked up only after 3 h. The results were identical to those reported above.

The absence of methylene bridge hydrogen exchange was substantiated by recording the ^{1}H-NMR and ^{2}H-NMR spectra of a [1.1]ferrocenophane which was deuterated selectively at one of the bridges (1-D-[1.1]ferrocenophane). This material was prepared by proton abstraction from FCP by butyl lithium (generating the bridge carbanion, which is stabilized by a C–H–C hydrogen bond [18]) and quenching with D_2O. The ^{1}H-NMR spectrum showed a signal at 3.53 ppm (3 H, singlet) for the bridge protons and the ferrocene multiplets at 4.32 ppm and 4.16 ppm (8 H each). The ^{2}H-NMR gave one signal at 3.55 ppm, and the mass spectrum gave m/e of 397 as the main peak.

The random distribution of deuterium in the α- and β-positions is further evidence for *exo*-attack of the electrophile. If a Fe–D species were formed first, the resulting structure **9**, in which the ring tilting is restricted to bending modes allowed by the CH_2 bridge, should be expected to show preferential deuterium transfer to the α-position. By contrast, *exo*-attack is not subject to such pre-coordination and therefore can be expected to be less regioselective and to produce a randomly ring-deuterated species.

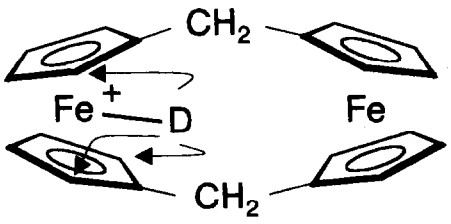

9

2.5. Dimeric [1.1]ferrocenophane ([1.1.1.1]ferrocenophane) (5)

In this cyclic tetraferrocene system, two of the opposing ferrocenes are quite close to each other, so that double protonation may be followed by dihydrogen elimination, yielding the bis-ferrocenium ion, and, after a second, reversible double protonation, to a tetracation **10**. Interestingly enough, the tetracation **10** now has two reaction choices. The first possibility is to again eliminate dihydrogen and to form the tetra-ferrocenium ion, which then no longer can be protonated. This H_2-elimination should be more difficult than the first one for reasons of Coulomb repulsion. The second possibility is electron transfer between the ferrocenium ions and ferrocenes in this structure to involve all four ferrocenes. The relative probabilities of these two reaction paths are hard to guess, because they involve solvated multiply charged species about which we know next to nothing.

The consequences of this choice, and which of them is preferred, should, however, be detectable in reactions with DBF_3OD: the first choice would lead to incomplete deuteration, due to rapid formation of the tetraferrocenium ions, whereas the second choice would lead to a (nearly) completely deuterated material, because an unlimited number of H/D exchange steps is possible.

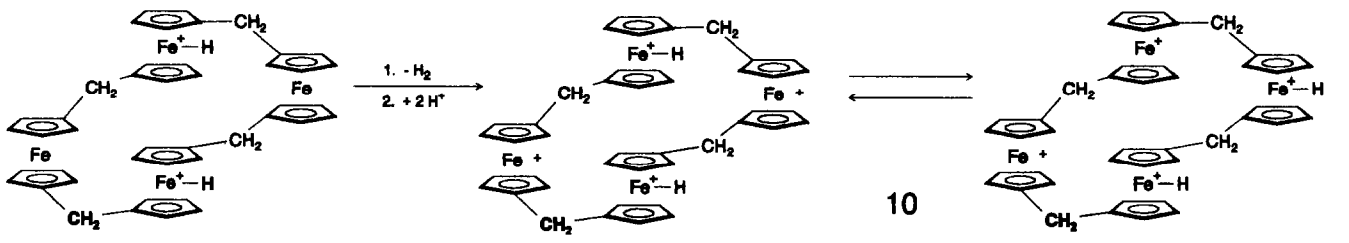

The dimer dissolved with rapid gas evolution in DBF_3OD, although the reaction qualitatively appeared somewhat slower than the nearly instantaneous reaction of the parent ferrocenophane. The solution turned blue and became green upon addition of water. Workup using the same procedures as for FCP gave back a yellow solid.

The ^{1}H-NMR spectrum showed the ferrocene protons as a broad multiplet at 4.0 ppm and the eight methylene protons as a singlet at 3.34 ppm with an integral close to 10:8. This means that 22 of the 32 ferrocene protons had exchanged. That approximately two-thirds of the hydrogens had undergone H/D exchange, whereas 50% of the hydrogens had been exchanged in the deuteration of [1.1]ferrocenophane, indicates a slightly slower reaction. This would be a expected from the conformational requirement that only opposing ferrocenes can eliminate dihydrogen, whereas adjacent ferrocenes will not take part in this step because they are too far apart. Because their protonation is just as likely as in any other of the four ferrocenes, the extent of deuteration would be expected to be higher.

Interesting information, which indeed indicated the existence of two reaction pathways came from the mass spectrum (Fig. 6) which showed a bimodal distribution of peaks. The main peak at *m/e* 824 corresponds to the fully deuterated ferrocenophane (d_{32}) and is accompanied by an exponentially diminishing group of lesser deuterated species, and by the typical peaks reflecting the same isotopic distributions seen in FCP and in the undeuterated FCP dimer. A second series of peaks, centered at *m/e* 814, showed the same Gaussian-type distribution we had observed in the reaction of FCP. The center of this group of peaks at *m/e* 814 corresponds to the d_{22} species.

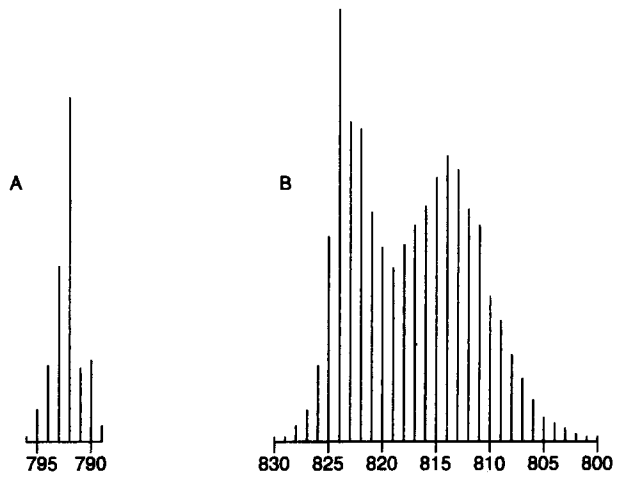

Fig. 6. Mass spectra of [1.1.1.1]ferrocenophane: (a) undeuterated and (b) after reaction with DBF_3OD and reductive work-up.

The intensity ratios do not allow a good estimate of the relative reaction rates in these two pathways, but the MS and NMR data taken together indicate that the first choice is preferred. We can envision this in slightly greater detail: the bis-ferrocenium ion, resulting from double protonation of opposite ferrocenes and hydrogen elimination, will want to rearrange itself such that the ferrocenium ions get further away from each other, forcing the two neutral ferrocenes to come closer together into a position where protonation is followed by hydrogen elimination [43]. The isostructural ring system containing two ferrocenes and two cobaltocenium ions was structurally characterized by X-ray diffraction and shows precisely this arrangement [11]. Its protonation has never been studied.

2.6. The mixed [1.1]ferroceno-ruthenocenophanes 4 and 6

A series of protonation or deuteration reactions of the mixed metallocenophane **4** and of its dimer **6** were undertaken to probe the details of the reactions of these compounds that have the same structures but different redox properties than the ferrocenophanes. Deuteration of these compounds, using DBF_3OD, was expected to provide further insight into the involvement of the metal and Cp rings during the protonation of these metallocenes and [1.1]metallocenophanes.

2.7. [1.1]Ferroceno-ruthenocenophane (4) in HBF_3OH and DBF_3OD

As postulated in the Introduction, a [1.1]metallocenophane must have a 2 + oxidation state available in order to be able to release dihydrogen from the diprotonated species. Where this 2 + state does not exist, the reaction should stop at the stage of protonation because the dissociation to dihydrogen and the metallocenophane dication would be energetically unfavorable.

Since ruthenocene does not undergo a one-electron oxidation, but is oxidized irreversibly to Cp_2Ru^{2+} in a two-electron step, the mixed [1.1]ferroceno-ruthenocenophane **5** can be oxidized to a monocation and a trication (see CV data in Table 1) — but a dication does *not* exist. It would therefore be reasonable to expect protonation of **4** to stop prior to hydrogen evolution unless an oxidizing agent is present which would allow access to the 3 + state and thus allow transient formation of the 2 + oxidation state. The reaction of [1.1]ferroceno-ruthenocenophane with HBF_3OH therefore is an especially interesting case to test the hypothesis that hydrogen evolution should not be possible in the metallocenophane due to the unavailability of a 2 + oxidation state.

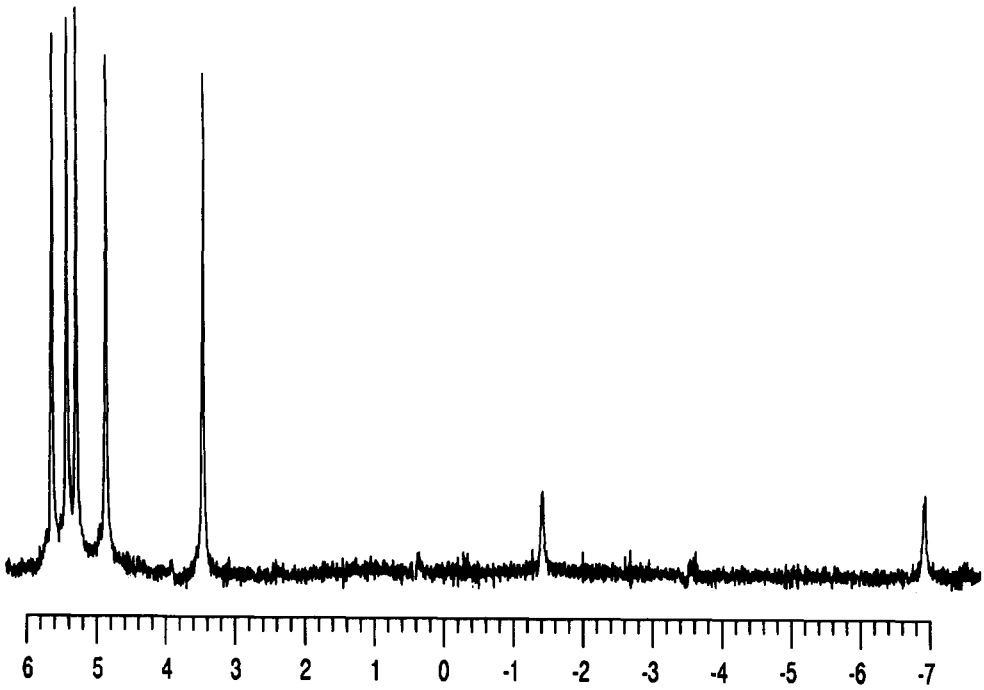

Fig. 7. 270 MHz ^{1}H-NMR spectrum of [1.1]ferroceno-ruthenocenophane **4** in HBF_3OH.

When crystalline [1.1]ferroceno-ruthenocenophane was added to HBF_3OH under nitrogen or argon, it dissolved immediately without any noticeable color change. This solution remained unchanged for more than 30 min and no gas evolution was observed. When the solution was exposed to air, it turned blue/green, indicating oxidation of the [1.1]metallocenophane.

The ^{1}H-NMR spectrum (Fig. 7) proved that the golden-yellow solution indeed contained the diprotonated species. In the spectrum taken at 270 MHz the ruthenocene multiplets appeared at 5.65 and 5.44 ppm, the ferrocene multiplets at 5.31 and 4.88 ppm, and the methylene bridges at 3.49 ppm as a singlet. The hydridic protons were observed at -1.48 and -6.9 ppm as slightly broadened singlets. Whereas the hydridic signal on protonated Cp_2Ru normally (see Fig. 2) appears as a sharp singlet, in this case it is as broad as the Fe–H signal. This may be due to the particular steric constraints of this system, to coupling between the two hydridic protons, or to traces of oxygen in the sample tube. When air was intentionally allowed to enter the NMR tube, the signals for the hydridic protons disappeared quickly. The metallocene and bridge signals became broad and the upfield protons were barely discernible, indicating the presence of a paramagnetic species and partial decomposition. Gas bubbles were observed in the NMR tube and the solution became green. Nevertheless, the starting material was recovered almost quantitatively by aqueous borohydride treatment and extraction with methylene chloride.

To observe the behavior of [1.1]ferroceno-ruthenocenophane in a deuterated acid, the 60 MHz ^{1}H-NMR spectrum of a solution of **4** in DBF_3OD was recorded within 2 min after preparing the solution in an argon purged NMR tube. The spectrum showed a signal at 8.30 ppm for the acid and three other signals: two multiplets of equal intensity were found at 5.40 and 5.60 ppm and a singlet at 3.50 ppm. The singlet had the same integral as the two multiplets. This result is as expected from what we just described in the reactions of ferrocene and ruthenocene with DBF_3OD and of the mixed metallocenophane with HBF_3OH: complete H/D exchange at the ferrocene, no exchange on the ruthenocene or at the bridge, and no gas evolution.

The d_8-[1.1]ferroceno-ruthenocenophane, completely and selectively deuterated on the ferrocene half, was recovered by aqueous sodium borohydride treatment and extraction with methylene chloride. The mass spectrum of the product showed a peak at *m/e* 449, 8 units above that of the non-deuterated [1.1]ferroceno-ruthenocenophane and thus confirmed the ^{1}H-NMR data. Whereas in [1.1]ferrocenophane the H/D exchange is incomplete due to the formation of the bis-ferrocenium ion and H_2, the complete deuteration for the ferrocenyl moiety of [1.1]ferroceno-ruthenocenophane has to be a result of the inability of this material to evolve hydrogen and of the reversible na-

ture of *exo*-ring attack of the electrophile seen in the [1.1]ferrocenophane investigation.

2.8. The dimeric [1.1]ferroceno-ruthenocenophane (6)

In this [1.1.1.1]metallocenophane the ferrocenes and the ruthenocenes occupy alternate positions in the ring with the opposing metallocenes facing each other and in relatively close contact. Cyclic voltammetry shows the first two oxidations to be centered on the ferrocenes. This system therefore has a 2+ state available and should be able to evolve hydrogen, albeit — due to the somewhat larger Fe–Fe distance — more slowly than [1.1]ferrocenophane, when it is dissolved in HBF_3OH.

Precisely this is observed experimentally. Dissolving the dimer in HBF_3OH in a nitrogen-purged vessel leads to slow and continuous gas evolution for more than 30 min. No attempt was made to record the NMR spectrum. The starting material was recovered by $NaBH_4$(aq) treatment and extraction with methylene chloride.

This reaction is much slower that what we observed for the isostructural ferrocenophane dimer described above as reacting rapidly and with gas evolution. The explanation for this observation is straightforward, if we look at the details of protonation and hydrogen elimination and of their consequences. In the tetraferrocene system, the double protonation of opposing ferrocenes, followed by dihydrogen elimination and rearrangement as discussed, generates the favorable conformation with the two neutral ferrocenes in proximity, which allows the second double protonation to generate the second molecule of hydrogen and the tetraferrocenium ion. In contrast to this situation, all of the metallocenes in the mixed ferrocene-ruthenocene dimer can be protonated, with the protonated ruthenocenes generating an unfavorable steric situation for elimination of dihydrogen from the two protonated ferrocenes. The net results is a very slow reaction.

We cannot directly extrapolate back from these results to the relative rates of protonation and hydrogen elimination in the parent ferrocenophane. However, we can conclude that protonation appears to be rapid in all the cases we studied and that hydrogen evolution is instantaneous unless steric or electronic factors prohibit it.

2.9. Electron transfer effects

In the reaction of [1.1]ferrocenophane and its analogs with acids we start with the neutral species and end up with the dication, according to the equation $FCP + 2H^+ \rightarrow FCP^{2+} \rightarrow H_2$. This overall equation is deceptively simple and it is clear that the reaction progresses through several intermediates. Only when, after dihydrogen elimination, the bis ferrocenium ion is formed and solvated in the reaction medium, it no longer participates directly in the reaction, because ferrocenium ions cannot easily be substituted or protonated. We must, however, suspect that it will react with neutral FCP to form the monocation through the conproportionation reaction $FCP + FCP^{2+} \rightarrow 2FCP^+$ and that it thus may play some role in the overall mechanism. In this particular system the kinetics must be expected to be complex, because we are facing a reaction between a viscous liquid and a dissolving solid, which becomes soluble only by reaction with the acid solvent. In addition, electron transfer in the solid, at the solid/liquid interface and in solution will contribute with quite different relative weights. Such kinetics are too difficult to tackle, and simple attempts to interpret them seem doomed to failure.

On the molecular scale, the overall process may be envisioned as follows: a [1.1]ferrocenophane molecule at the surface of the crystal is protonated once and then (i) either diffuses into the acid to be protonated again, evolve dihydrogen, and form the dication, or (ii) it is protonated a second time while still in contact with the solid; then it either diffuses away or loses dihydrogen before doing so; all of the cationic species can pick up an electron from an adjacent neutral molecule in the solid; the unprotonated monocations may diffuse into the acid solution and two of them might also disproportionate to the dication and the neutral species. The potential coexistence of conproportionation and disproportionation is not contradictory, because they would occur in different environments, in solution or at the solid/liquid interface. We have no data to support any mechanistic details on intermolecular electron transfer, but we know quite precisely the consequences of such equilibria. From these we conclude that there are indeed several indications that intermolecular electron transfer occurs in these reactions.

When ferrocenophanes react with deuterated acid, the monocations, resulting from electron transfer, play a significant role in the degree of deuteration. The key point is that they can be protonated but cannot eliminate dihydrogen: double protonation of the monocation would generate a triply charged species, and loss of H_2 would leave a trication behind; there is, however, no evidence in the cyclic voltammograms of [1.1]ferrocenophane for the existence of such a trication at any reasonable potential. These monocations are therefore doomed to undergo H/D exchange without hydrogen evolution stopping this process. The protonation of the monocation leads to the dication $H–FCP^{++}$ with a relatively high oxidation potential which

would allow the oxidation of neutral FCP to the monocation ($H-FCP^{2+} + FCP \rightarrow H-FCP^{+} + FCP^{+}$) to occur.

This helps us understand the degree of deuteration. It is only possible to interpret these results if protonation (or deuteration) occurs *via exo*-attack and if it involves a rapid equilibrium between C–H and Fe–H species. Unless, like in the case of the parent [1.1]ferrocenophane, the overall rate is very high, the species in question can be reversibly protonated many times on either of its ferrocenes. In deuterated acid this means complete deuteration for slow overall reactions and partial deuteration in the case of very rapid processes. In the fast reaction case, we also find evidence for the importance of electron transfer, because in this case more than a statistical amount of *undeuterated* [1.1]ferro-cenophane is detected upon workup. The only way this species can be formed is the reaction of a neutral molecule with one of the cations to go directly to the unreactive dication without undergoing deuteration and H_2 (or HD and D_2) evolution.

Whereas this sequence of reactions permits us to interpret the experimental results in a consistent way, we should also keep in mind that significant deuteration would also result, even in the absence of electron transfer, if the last reaction step (hydrogen elimination) would be rate limiting: the first and second deuteration can then occur many times before the slow step brings the system into the irreversible regime where the two ferrocenium ions arrest further H/D exchange. This interpretation has been proposed by Hillman [41], based on his kinetic data. In view of the much more complex nature of this reaction and the additional information we present here, it is clear that Hillman's work is based on assumptions about the nature of the intermediates and reaction products which might have to be revised. In particular, the role of the carbocations in reactions involving more dilute acids was not recognized the previous work.

2.10. [1.1]Ferrocenophane reactions under reducing conditions

We were surprised to discover that the addition of a very small amount of tin or lead metal to the reaction of [1.1]ferrocenophane with DBF_3OD, the NMR and MS data showed that complete ring deuteration had occurred. If more than one equivalent of reductant were involved, this would be no surprise, because [1.1]ferrocenophane acts as a catalyst with many turnovers in the reaction of these metals with the deuterated acid, but we found that only a fraction of one equivalent of metal was sufficient to effect complete exchange.

One postulate to explain these observations would be the presence of an abnormally large isotope effect in the protonation step, but this is not satisfactory, because there would be no obvious reason for such an effect and, if it existed, it could account at best for enhanced exchange but not for complete deuteration. The absence of any unusual isotope effect was, furthermore, indicated by the reaction of the completely ring deuterated system (d_{16}–FCP) with HBF_3OH. The ^1H-NMR spectrum of the purified reaction product showed a bridge proton to ring proton ratio of approximately 4:3:3. The mass spectrum showed the maximum peak at 402, denoting the incorporation of, on average, six hydrogens for deuterium (about 40% H/D exchange). This corresponds to a normal isotope effect.

The reaction of FCP^{2+} with Sn may proceed in two one-electron redox steps or *via* one two-electron redox

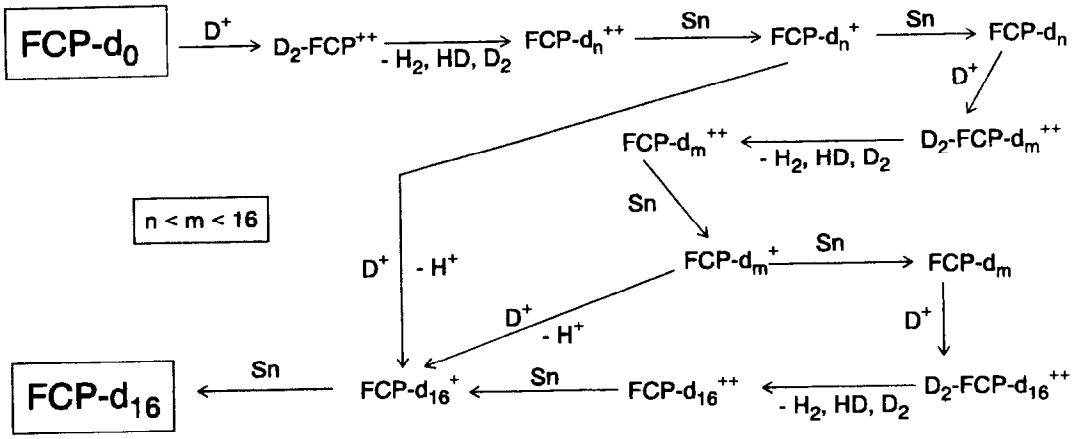

Fig. 8. Complete deuteration of FCP in DBF_3OD under reducing conditions. The non- or partially deuterated FCP-monocation is the crucial intermediate to effect complete deuteration by one of several pathways.

process. In either case, the possibility of electron transfer (con- or dis-proportionation) between the 0, 1+ and 2+ charged [1.1]ferrocenophane species must be considered. If the neutral [1.1]ferrocenophane would be formed in solution, it would react with the acid in the usual way but with kinetics different from those seen for the reaction of solid FCP with acid, and intermolecular electron transfer could equilibrate this species with the mono- and dication. Formed either in this way or by a one-electron reduction of the [1.1]ferrocenophane dication, the monocation FCP^+ is the crucial intermediate (Fig. 8).

Once the monocation is formed, it cannot, as we saw above, contribute to the hydrogen evolution. It can, however, undergo many protonation/deprotonation steps and will, in deuterated acid, undergo complete H/D exchange. This done, it can transfer an electron to another dication and set it up for H/D exchange. A chain of these reactions easily accounts for complete deuteration of the entire batch before the reduction ends. It explains the need for only minute amounts of reductant to have this effect.

It is thus the unprotonated mono-cation (ferrocenophanium ion) and not the mono-protonated ferrocenophanonium ion which is mainly responsible for H/D exchange. Once the mono-protonated ion picks up a second proton, the resulting diprotonated species loses dihydrogen immediately and forms the bis-ferrocenium ion. This mechanism is intuitively plausible and finds support in the results presented here.

3. Summary and conclusions

One portion of this work has been a reinvestigation of long known reactions such as the protonation of ferrocene and ruthenocene, about which some confusion has existed in the literature especially in regard to the exact mechanism of this process. It is now unequivocally clear that the protonation of ferrocene proceeds *via exo* attack and that it involves a rapid equilibrium between ring and Fe–H protonated species. As a consequence, the observed NMR spectrum actually represents an average of these extremes and complete and rapid deuteration of the rings occurs in deuterated acids. In ruthenocene, the rings do not participate in the protonation and the existence of only the Ru–H species is seen in the NMR spectrum and in the absence of any detectable ring deuteration in reactions with deuterated acids. This is in accord with semi-empirical MO calculations but also poses a problem for more sophisticated quantum chemical approaches.

The results from the deuteration of ferrocenophane and of the mixed Fe–Ru analog give new and additional evidence for these pathways of protonation. In [1.1]ferrocenophanes, the protonation leads to elimination of dihydrogen and the formation of the bis-ferrocenium ion. The rate limiting step in this reaction seems to be the second protonation: as soon as the second proton is attached, the hydrogen elimination can proceed. From the reaction in DBF_3OD we can learn that approximately eight deuteration–deprotonation reactions occur before H_2 elimination generates the bis-ferrocenium ion, which then no longer is subject to H/D exchange.

The reaction of the [1.1]ferroceno-ruthenocenophane with DBF_3OD leads to complete deuteration of the ferrocene portion but no H/D exchange is detected for the ruthenocene half and the bridges. The mixed Fe–Ru system can be protonated twice, but it cannot eliminate dihydrogen. This is due to the fact that this compound can be oxidized to a 1+ and a 3+ ion but not to a 2+ cation. The inaccessibility of a 2+ oxidation state does not allow elimination of dihydrogen from the diprotonated species. The diprotonated species lives long enough to be observed by NMR: we can identify the Ru–H and the Fe–H signals.

In the dimeric systems with four ferrocenes or two ferrocenes and two ruthenocenes we observe two very different protonation rates. In the ferrocenophane dimer, two successive double protonations and dihydrogen eliminations are possible, but a secondary reaction path, involving incomplete protonation is also involved. In deuterated acid, the two choices can be distinguished, because the latter path leads to complete H/D exchange, whereas the main path produces a partially deuterated product. The mixed dimer also shows hydrogen evolution, but in this case this is an unfavorable and slow process involving a sterically awkward tri- or tetra-protonated species.

For the [1.1]ferrocenophane, the mono-ferrocenium ion makes important contributions in complete H/D exchange reactions. It can be protonated, but it cannot be removed from H/D exchange through dihydrogen elimination. The formation of the mono-ferrocenium ion by conproportionation of neutral FCP and the FCP dication or by other redox processes explains the complete deuteration observed under reducing conditions.

4. Experimental details

Reagents were obtained from either Fisher, Alfa, MCB, Matheson, or Aldrich Chemical Companies. All reactions were routinely carried out under positive pressure of nitrogen in multineck flasks. Tetrahydrofuran (THF) and hexane were distilled from lithium aluminum hydride or sodium benzophenone ketyl before each use. Tetramethylethylenediamine (TMEDA) was distilled and stored under nitrogen. Acetonitrile

was distilled twice from phosphorus pentoxide. Dioxane was stored over potassium hydroxide, and distilled from sodium metal after 24 h of reflux. Other solvents were the best commercial grade and were used without purification, except where noted. Ferrocene was purified by continuous extraction with hexane through an Al_2O_3 column. Ruthenocene was recrystallized from hexane. The 270 MHz ^{1}H-NMR spectra were obtained on a Bruker/IBM AF-270 spectrophotometer. The 60 MHz ^{1}H-NMR spectra were obtained on either a Varian T-60 NMR spectrometer or a Varian EM360-A NMR spectrometer. The ^{2}H-NMR spectra were obtained on Bruker WH-90 instrument. Infrared spectra were obtained on a Perkin-Elmer 238 spectrophotometer. Mass spectral determinations were made on a Kratos MS-902 high-resolution, double-focusing mass spectrometer. Elemental analyses were obtained at MICANAL Laboratories, Tucson, AZ. Melting points were determined on a Mel-Temp (Lab Devices) and are uncorrected.

4.1. Syntheses

[1.1]Ferrocenophane, [1.1]ferroceno-ruthenocenophane, and [1.1]ruthenocenophane were prepared according to literature procedures [1–6]. The dimeric systems [1.1.1.1]ferrocenophane (5) and [1.1.1.1]ferroceno-ruthenocenophane (6) were isolated as by-products of these syntheses. Their preparations are described below.

4.1.1. HBF_3OH and DBF_3OD

Boron trifluoride hydrate was prepared from boron trifluoride and water. In a 50 ml round-bottomed flask, approximately 3–5 ml H_2O were heated to boiling while a stream of nitrogen was passed through the liquid to remove oxygen. The flask was cooled under nitrogen in an ice-methanol bath, boron trifluoride was bubbled into the water until the solution was saturated. The temperature was not allowed to rise above 0°C. The solution was protected from air and moisture and used immediately. DBF_3OD was prepared in an analogous fashion using D_2O.

4.1.2. [1.1]Ferrocenophane and [1.1.1.1]ferrocenophane

A change from the literature procedure [3] was made in the workup. After the reaction mixture was stirred for an hour, a small amount of water (about 3 ml) was added to hydrolyze the reaction mixture. A green sludge appeared. This mixture was filtered under nitrogen into a 1.5 l Erlenmeyer flask and dried with $MgSO_4$. The clear orange solution was filtered, the solvent was evaporated, and the residue was dissolved in the minimum amount of CCl_4. In the hood, an Al_2O_3/CCl_4 column was prepared by attaching a nitrogen line to the bottom of the column (6 × 60 cm) and adding CCl_4 to three-fourths the height of the column while a rapid nitrogen flow was maintained during the addition of Al_2O_3(basic II). The nitrogen flow was then stopped and the Al_2O_3 was allowed to settle. Washed sea sand (about 2 cm) and then the reaction mixture were placed on top of the column. Elution with CCl_4 was allowed to go as rapidly as the column allowed. The first two zones were collected. The solvent from the first zone was evaporated, and the golden-yellow crystalline [1.1]ferrocenophane was recrystallized from heptane. The second zone gave the [1.1]FCP dimer as an orange solid, which was recrystallized from acetone. The purity of [1.1]FCP was checked by melting point, (222°C; lit. [3] 223°C), ^{1}H-NMR, and mass spectroscopy. The [1.1.1.1]ferrocenophane darkened at 255°C. The ^{1}H-NMR spectrum showed a broad multiplet at 4.01 (32 H) for the ferrocene protons. The bridge proton signal was found at 3.31 ppm (8 H, singlet). The mass spectrum gave a main peak at *m/e* 792.

4.1.3. Exo–exo- and exo–endo-1,12-dimethyl[1.1]ferrocenophane

The mixture of isomers was prepared according to the literature [3] from 1,1′-bis-(6-fulvenyl)-ferrocene. The workup was carried out using the same modifications noted above for [1.1]ferrocenophane. The combined eluents of the first chromatography on Al_2O_3 were evaporated, the residue taken up in a small amount of CCl_4 and chromatographed on a silica gel column with CCl_4. The first two zones were collected (the second zone contains a mixture of the dimers). The first zone was evaporated, and a crystalline mixture of the two isomers remained. This solid was fractionally recrystallized from heptane. The *exo–exo* 1,12-dimethyl[1.1]ferrocenophane crystallized first to give a golden-yellow solid. Its purity was checked by melting point, 183°C (lit.: [see Ph.D Thesis TJH] 185–186°C), and ^{1}H-NMR. The 270 MHz ^{1}H-NMR spectrum in $CDCl_3$ showed two multiplets for the ferrocene protons at 4.59 ppm (4 H) and 4.16 ppm (12 H) and a quartet for the bridge protons at 3.75 ppm (2 H, $J = 7$ Hz). The signal for the methyl protons was found at 1.17 ppm (6 H, $J = 7$ Hz). The heptane supernatant was evaporated from the filtrate leaving the *exo–endo* isomer. This isomer was recrystallized from a minimal amount of hexane (about 5 ml). The melting point of the *exo–endo* isomer was 105°C (lit.: [3] 109°C). The 270 MHz ^{1}H-NMR spectrum in $CDCl_3$ showed two multiplets for the ferrocene protons at 4.10 ppm (8 H) and 4.20 ppm (8 H) and a quartet for the bridge protons at 3.61 ppm (2 H, $J = 7$ Hz). The signal for the methyl protons was found at 1.21 ppm (6 H, $J = 7$ Hz).

4.1.4. Exo–exo 1,12-Dimethyl[1.1]ferrocenophane from [1.1]ferrocenophane

In this "one-pot" synthesis utilizing the red bridge carbanions of FCP and 1-methyl-FCP [18], [1.1]ferrocenophane (0.25 g, 0.63 mmol) and THF (50 ml), were placed in a nitrogen-purged 3-neck, 500 ml round-bottom flask with a stirring bar. The flask was placed into an ice-methanol bath. To a 60 ml pressure equalizing dropping funnel affixed to one neck of the flask, THF (40 ml) was added along with methyl iodide (1 ml, 15.0 mol). To a second funnel, hexane (40 ml) was added together with n-butyllithium (2.2 M, 2 ml, 4.4 mmol). One equivalent of n-butyllithium (6.0 ml, 0.63 mmol) was added to the solution, and the resulting red solution was stirred for about 10 min. The methyl iodide solution was added a drop at a time until the reaction solution became yellow. This solution was stirred for 2 min, and if it became darker, another drop of methyl iodide was added. This was continued until a color change was no longer observed. (If the reaction was terminated at this time, the 1-methyl[1.1]ferrocenophane derivative could be isolated using the same workup procedures in [1.1]FCP synthesis.) The same sequence of additions was repeated a second time. The yellow reaction mixture was hydrolyzed with a small amount of water (1 ml), and a white precipitate formed. The mixture was filtered and the solvent was evaporated. The residue was chromatographed over a short Al_2O_3/CCl_4 column and the first band was collected. The solvent was evaporated, and the yellow solid was recrystallized from hexane to give *exo–exo*-1,12-dimethyl[1.1]ferrocenophane. The purity of the *exo–exo*-[1.1]FCP was checked by TLC (one spot) and ^{1}H-NMR. The 270 MHz 1H-NMR spectrum was consistent with the spectrum of the known material. The yield was 0.21 g (78%).

4.1.5. Deuteration at the methylene bridge of [1.1]ferrocenophane

[1.1]Ferrocenophane (100 mg, 0.25 mmol) was added to THF (10 ml) in an ice cooled nitrogen-purged round-bottom flask with a stirring bar. n-Butyllithium (1.2 M, 0.50 ml, 0.60 mmol) was added to the flask *via* a syringe. The solution turned immediately to dark red. D_2O (0.50 g, 0.25 mol) was added to quench the reaction. The solution turned back to yellow and produced a small amount of white precipitate. The solution was evaporated, the yellow solid was extracted with methylene chloride, the solution washed with water, dried, and evaporated. Recrystallization from hexane gave the mono-bridge-deuterated derivative of [1.1]FCP. The ^{1}H-NMR gave signals for the bridge protons at 3.53 ppm (3 H, singlet) and ferrocene multiplets at 4.32 ppm (8 H) and 4.16 ppm (8 H). The ^{2}H-NMR gave one peak at 3.55 ppm (1 D, singlet). The mass spectrum gave the main peak at *m/e* 397.

4.2. Reactions with acids

4.2.1. Deuteration of [1.1]ferrocenophane by DBF_3OD

Solid [1.1]ferrocenophane (100 mg, 0.25 mmol) was added to DBF_3OD. The solution turned blue, then blue/green while H_2 was evolved. Water was added and the green material was extracted into methylene chloride ($\lambda_{max} = 740$ nm). An aqueous solution of sodium borohydride (about 250 mg $NaBH_4$ in 5 ml water) was added to the CH_2Cl_2, and the solution turned yellow. The CH_2Cl_2 layer was removed, and the H_2O layer was washed with CH_2Cl_2 until it was colorless. The CH_2Cl_2 extract was dried with $MgSO_4$, and the solvent was evaporated, leaving a golden-yellow crystalline solid. The ^{1}H-NMR spectrum showed the bridge protons at 3.53 ppm (4 H, singlet) and the ferrocene protons at 4.32 ppm (n 4 H, multiplet) and 4.16 ppm (n 4 H, multiplet). The mass spectrum showed the main peak at *m/e* 404 with a Gaussian distribution. There was a statistically significant signal at 396 (FCP-d_0). The ^{2}H-NMR gave only one broad peak at 4.31 ppm.

4.2.2. Deuteration of [1.1]ferrocenophane by DBF_3OD in the presence of excess Pb or Sn

[1.1]Ferrocenophane (100 mg, 0.25 mmol) was added to DBF_3OD along with tin metal (25 equivalents of Sn, 0.39 g, 3.2 mmol). Lead was also used in place of the tin for a follow-up experiment with identical results. The solution turned blue and evolved hydrogen almost immediately upon the addition. The gas evolved for 180 min with very slow consumption of the Sn metal. The reaction was stopped at this time by diluting the solution with water, and the green material was extracted into methylene chloride. The same workup was carried out as in the [1.1]FCP deuteration. The electronic spectrum of the blue solution gave transitions at 640 nm, 560 nm, and 465 nm. The electronic spectrum of the green solution gave broad transitions at 745 nm and 460 nm. The 270 MHz ^{1}H-NMR spectrum gave a bridge proton signal at 3.52 ppm (4 H, singlet) and no signal where one would expect ferrocene protons. The 90 MHz ^{2}H-NMR spectrum gave one signal at 4.32 ppm. The mass spectrum showed a main peak at *m/e* 412.

4.2.3. Deuteration of [1.1]ferrocenophane by DBF_3OD in the presence of substoichiometric amounts of Sn

Four reactions, one using 5 equiv. (0.075 g, 0.63 mmol), one using 2 equiv. (0.03 g, 0.076 mmol), one

using 1 equiv. (0.015 g, 0.038 mmol), and the last using only one grain of Sn and [1.1]ferrocenophane (100 mg, 0.25 mmol) were conducted using the same procedures as outlined in the above deuteration using 25 equivalents of Sn. All of the solutions turned blue and evolved gas almost immediately upon the addition of the [1.1]FCP. The gas evolved for 180 min with very little consumption of the Sn metal in each of the reaction flasks. The reactions were terminated after 180 min had elapsed, except for the flask containing one grain. That reaction was allowed to proceed for an additional 60 min. The slow evolution of gas was still observed after the additional hour. Workup was carried out as before. The spectroscopic data was the same as before.

4.2.4. Protonation of d_{16}-[1.1]ferrocenophane by HBF_3OH

d_{16}-[1.1]Ferrocenophane (100 mg, 0.25 mmol) was added to HBF_3OH. The solution turned blue, then green almost immediately. After stirring for 5 min, H_2O was added to dilute the acid. Workup was carried out as before. The 270 MHz ^{1}H-NMR spectrum gave signals for the bridge protons at 3.53 ppm (4 H, singlet) and the ferrocene protons at 4.32 ppm (n 3 H, multiplet) and 4.16 ppm (n 3 H, multiplet). The mass spectrum showed the main peak at *m/e* 396.

4.2.5. Protonation of [1.1]ferroceno-ruthenocenophane by HBF_3OH

In a nitrogen-purged NMR tube, crystals of [1.1]ferroceno-ruthenocenophane (50 mg, 0.11 mmol) were agitated by a gentle flow of nitrogen in order to purge the solid of any adsorbed oxygen. Upon addition of HBF_3OH, the solid dissolved immediately, resulting in a deep yellow solution. No gas evolution was observed. The 270 MHz ^{1}H-NMR spectrum is reproduced as Fig. 7. A large water peak was found at 8.30 ppm. All of the chemical shift data were taken relative to the water signal to be consistent with the other reactions.

4.2.6. Deuteration of [1.1]ferroceno-ruthenocenophane by DBF_3OD

A small amount of [1.1]ferroceno-ruthenocenophane ($\approx$ 25 mg, 0.06 mmol) was added to DBF_3OD. The yellow solid went directly into solution. Gas evolution was not observed. The solution was filtered into a nitrogen-purged NMR tube. The spectrum showed the signals for the methylene bridge protons at 3.60 ppm (4 H) as a singlet and the ruthenocene signals at 5.65 and 5.44 ppm as multiplets (4 H each). A water peak was found at 8.30 ppm. The ferrocene signals had disappeared. Spectra were rerun at 2, 10, 15, and at 30 min. When the solution was allowed contact with the atmosphere, the solution became intensely green and gas evolution was observed, lasting for about 3 min. Workup was conducted as in the [1.1]ferrocenophane deuteration. The mass spectrum showed a main peak at *m/e* of 449.

4.2.7. Deuteration of [1.1.1.1]ferrocenophane by DBF_3OD

The [1.1]ferrocenophane dimer (50 mg, 0.06 mmol), as a yellow-orange solid, was added to DBF_3OD. The solid dissolved rapidly, resulting in first a blue-green solution and in evolution of H_2 gas. After stirring the solution for 5 min, water was added, but no color change was observed. Aqueous sodium borohydride reduction and workup was carried out as in the [1.1]FCP deuteration, and hexane extraction gave an orange solid. The electronic spectrum of the dimer showed a transition at 430 nm. The blue-green solution showed transitions at 620 nm and 470 nm. The 270 MHz ^{1}H-NMR spectrum showed a signal for the bridge protons at 3.31 ppm (8 H, singlet). The signal for the ferrocene protons was found as a broad multiplet at 4.00 ppm (n 10 H). The bimodal mass distribution of the mass spectrum is shown in Fig. 6.

References and notes

1 A. Cassens, P. Eilbracht, U.T. Mueller-Westerhoff, A. Nazzal, M. Neuenschwander and W. Prössdorf, *J. Organomet. Chem., 205* (1981) C17.
2 U.T. Mueller-Westerhoff, A. Nazzal and W. Prössdorf, *J. Organomet. Chem., 205* (1981) C21.
3 A. Cassens, P.E. Eilbracht, A. Nazzal, W. Prössdorf and U.T. Mueller-Westerhoff, *J. Am. Chem. Soc., 103* (1981) 6367.
4 U.T. Mueller-Westerhoff, A. Nazzal and M. Tanner, *J. Organomet. Chem., 236* (1982) C41.
5 T.J. Haas and U.T. Mueller-Westerhoff, *Synth. React. Inorg. Met. Org. Chem., 22* (1992) 227.
6 U.T. Mueller-Westerhoff and G.F. Swiegers, *Synth. React. Inorg. Met. Org. Chem., 23* (1993) 589.
7 M.F. Moore, S.R. Wilson, D.N. Hendrickson and U.T. Mueller-Westerhoff, *Inorg. Chem., 23* (1984) 2918.
8 M.F. Moore, S.R. Wilson, M.J. Cohn, T.Y. Dong, U.T. Mueller-Westerhoff and D.N. Hendrickson, *Inorg. Chem., 24* (1985) 4559.
9 U.T. Mueller-Westerhoff, G.F. Swiegers and A.L. Rheingold, *Angew. Chem., 104* (1992) 1398; *Angew. Chem., Int. Ed. Engl., 31* (1992) 1352.
10 A.L. Rheingold, U.T. Mueller-Westerhoff and G.F. Swiegers, *Organometallics, 11* (1992) 3411.
11 R.F. Kirchner, G.H. Loew and U.T. Mueller-Westerhoff, *Theor. Chim. Acta, 41* (1976) 1.
12 M.C. Zerner, G.H. Loew, R.F. Kirchner and U.T. Mueller-Westerhoff, *J. Am. Chem. Soc., 103* (1980) 589.
13 A. Waleh, M.L. Cher, G.H. Loew and U.T. Mueller-Westerhoff, *Theor. Chim. Acta (Berl.), 64* (1984) 167.
14 A. Waleh, G.H. Loew and U.T. Mueller-Westerhoff, *Inorg. Chem., 23* (1984) 2859.
15 V.K. Kansal, W.E. Watts, U.T. Mueller-Westerhoff and A. Nazzal, *J. Organomet. Chem., 243* (1983) 443.
16 A. Diaz, U.T. Mueller-Westerhoff, A. Nazzal and M. Tanner, *J. Organomet. Chem., 236* (1982) C45.

17 U.T. Mueller-Westerhoff, A. Nazzal, W. Prössdorf, J.J. Mayerle and R.L. Collins, *Angew. Chem., 94* (1982) 313; *Angew. Chem., Int. Ed. Engl., 21* (1982) 293; *Angew. Chem. Suppl.*, (1982) 686.
18 U.T. Mueller-Westerhoff, A. Nazzal and W. Prössdorf, *J. Am. Chem. Soc., 103* (1981) 7678.
19 U.T. Mueller-Westerhoff, *Angew. Chem., 98* (1986) 700; *Angew. Chem., Int. Ed. Engl., 25* (1986) 702.
20 U.T. Mueller-Westerhoff and A. Nazzal, *J. Am. Chem. Soc., 106* (1984) 5381.
21 T.J. Curphy, J.O. Santer, M. Rosenblum and J.H. Richards, *J. Am. Chem. Soc., 82* (1960) 5249.
22 M. Rosenblum, J.O. Santer and W.G. Howells, *J. Am. Chem. Soc., 85* (1963) 1450.
23 B. Floris, G. Illuminati and G. Ottaggi, *Tetrahedron Lett., 4* (1972) 269.
24 B. Floris, G. Illuminati, G. Ottaggi and P.E. Jones, *Coord. Chem. Rev., 8* (1972) 39.
25 G. Cerichelli, G. Illuminati, G. Ortaggi and A.M. Guiliani, *J. Organomet. Chem., 127* (1977) 357 and references cited therein.
26 S.P. Gubin, S.A. Smiranova, L.I. Denisovich and A.A. Lubovich, *J. Organomet. Chem., 30* (1971) 243.
27 T.E. Bitterwolf and A.C. Ling, *J. Organomet. Chem., 57* (1973) C15; T.E. Bitterwolf and A.C. Ling, *J. Organomet. Chem., 40* (1972) 197; T.E. Bitterwolf and A.C. Ling, *J. Organomet. Chem., 141* (1977) 355; T.E. Bitterwolf and A.C. Ling, *J. Organomet. Chem., 215* (1981) 77.
28 T.E. Bitterwolf, *Tetrahedron Lett., 22* (1981) 2627.
29 C.A. Burton and W.E. Watts *J. Chem. Soc., Perkin Trans. II*, (1983) 1591.
30 W.E. Watts, in G. Wilkinson, F.G.A. Stone and E.N. Abel (eds.), *Comprehensive Organometallic Chemistry*, Pergamon, New York, 1982.
31 A.F. Cunningham Jr., *J. Am. Chem. Soc., 113* (1991) 4864.
32 M.L. McKee, *J. Am. Chem. Soc., 115* (1993) 2818.
33 G. Wilkinson and J.M. Birmingham, *J. Am. Chem. Soc., 77* (1955) 3421.
34 P. Seiler and J.D. Dunitz, *Acta. Crystallogr., B35* (1979) 1068, 2020.
35 J.S. McKechnie, C.A. Maier, B. Bersted and I.C. Paul, *J. Chem. Soc., Perkin Trans. II*, (1973) 138.
36 R. Subra, A. Grand and U.T. Mueller-Westerhoff, unpublished results.
37 C. Park and J. Amlöf, *J. Chem. Phys., 95* (1991) 1829 and references cited therein.
38 M. Löwendahl, Ö. Davisson, P. Ahlberg and M. Håkansson, *Organometallics, 12* (1993) 2417.
39 (a) W.E. Watts, *J. Am. Chem. Soc., 85* (1966) 855; W.E. Watts, *J. Organomet. Chem., 10* (1967) 191; (b) T.H. Barr, H.L. Lentzner and W.E. Watts, *Tetrahedron, 25* (1969) 6001.
40 M. Hillman, S. Michaile, S.W. Feldberg and J.J. Eisch, *Organometallics, 4* (1985) 1258.
41 S. Michaile, M. Hillman and J.J. Eisch, *Organometallics, 7* (1988) 1059.
42 B.G. Gavini, T.J. Haas, K.L. Plourde and U.T. Mueller-Westerhoff, *Synth. React. Inorg. Met. Org. Chem., 22* (1992) 481.
43 A reviewer has suggested that a slowly or non-interconverting boat/chair conformational difference might be responsible for this effect. Although this idea is akin to our proposal, it suggests an additional, but hard to confirm, structural aspect. We thank the reviewer for this very constructive idea.